Hermetically Coated Superparamagnetic Fe_2O_3 Particles with SiO_2 Nanofilms

Alexandra Teleki,[†] Marcel Suter,[‡] Piran R. Kidambi,[†] Olgaç Ergeneman,[§] Frank Krumeich,[†] Bradley J. Nelson,[§] and Sotiris E. Pratsinis*,[†]

Particle Technology Laboratory, Micro- and Nanosystems, and Institute of Robotics and Intelligent Systems, Department of Mechanical and Process Engineering, ETH Zurich, Sonneggstrasse 3, CH-8092 Zurich, Switzerland

Received November 19, 2008. Revised Manuscript Received February 13, 2009

Magnetic nanoparticles are frequently coated with SiO_2 to improve their functionality and biocompatibility in a range of biomedical and polymer nanocomposite applications. In this paper, a scalable flame aerosol technology is used to produce highly dispersible, superparamagnetic iron oxide nanoparticles hermetically coated with silica to retain full magnetization performance. Iron oxide particles were produced by flame spray pyrolysis of iron acetylacetonate in xylene/acetonitrile solutions and the resulting aerosol was in situ coated with silicon dioxide by oxidation of swirling hexamethlydisiloxane vapor. The process allows independent control of the core Fe_2O_3 (maghemite) particle properties and the thickness of their silica coating film. This ensures that the nonmagnetic SiO_2 layer can be closely controlled and minimized. The optimal SiO_2 content for complete (hermetic) encapsulation of the magnetic core particles was determined by isopropanol chemisorption. The magnetization of Fe_2O_3 coated with about 2 nm thin SiO_2 layers was nearly identical to that of uncoated, pure Fe_2O_3 nanoparticles.

Introduction

Magnetic nanoparticles can bind to drugs, proteins, enzymes, antibodies, or nucleotides and can be directed to an organ, tissue, or tumor using external magnetic fields.[1] Though metallic nanoparticles such as Co, Ni, and Fe have a higher magnetization than metal oxides, they are highly reactive and toxic and, thus, less suitable for biomedical applications.[2] Iron oxide nanoparticles with appropriate surface chemistry have been widely investigated for in vivo applications such as magnetic resonance imaging (MRI) contrast enhancement, drug delivery, hyperthermia, and cell separation.[1,2] Further applications include humidity sensors[3] and magnetic, transparent nanocomposites.[4]

Superparamagnetic particles do not retain any permanent magnetization after removal of an applied magnetic field, thus facilitating their stability and dispersion.[1] This phenomenon occurs below a critical, material-dependent size when the thermal energy exceeds the magnetic anisotropy energy, i.e., the energy required to change magnetization direction, and thus the magnetization is easily flipped.[2,5,6] Such materials exhibit no hysteresis and the bulk material properties of remanence and coercivity vanish, e.g., those of bulk ferromagnetic γ-Fe_2O_3 (maghemite).[7] The magnetic moment of such superparamagnetic materials is much larger than those of paramagnetic materials.

Silica coating is often applied to magnetic Fe_xO_y nanoparticles to improve their functionality and biocompatibility.[2] Silica is stable in aqueous conditions and prevents magnetically induced self-agglomeration of magnetic cores. Silanol groups on the silica surface react with alcohols and silane coupling agents to produce stable dispersions in nonaqueous solvents and can be further modified by covalent bonding of specific ligands.[1] Furthermore, silica-coated or -embedded γ-Fe_2O_3 nanoparticles exhibit improved thermal stability. Pure or uncoated γ-Fe_2O_3 is thermally unstable and is transformed to hematite (α-Fe_2O_3), the most stable polymorph of iron(III) oxides, at high temperatures.[8] This transformation temperature is around 400 °C depending on particle size while ϵ-Fe_2O_3 can be formed as an intermediate in the transformation from γ-Fe_2O_3 to α-Fe_2O_3. This is observed especially for small particles at notably higher temperatures (500−750 °C for ϵ- to α-Fe_2O_3 transformation). Silica retards such transformations of γ-Fe_2O_3 to ϵ- or α-Fe_2O_3 in O_2 or air.[9,10] Silica-coated Fe_3O_4 nanoparticles functionalized by phosphorescent iridium complexes have three functionalities: MRI, luminescence imaging, and

* To whom correspondence should be addressed. E-mail: pratsinis@ptl.mavt.ethz.ch.
[†] Particle Technology Laboratory.
[‡] Micro- and Nanosystems.
[§] Institute of Robotics and Intelligent Systems.

(1) Gupta, A. K.; Gupta, M. *Biomaterials* **2005**, *26*, 3995.
(2) Lu, A. H.; Salabas, E. L.; Schuth, F. *Angew. Chem., Int. Ed.* **2007**, *46*, 1222.
(3) Sun, H. T.; Cantalini, C.; Faccio, M.; Pelino, M.; Catalano, M.; Tapfer, L. *J. Am. Ceram. Soc.* **1996**, *79*, 927.
(4) Ziolo, R. F.; Giannelis, E. P.; Weinstein, B. A.; Ohoro, M. P.; Ganguly, B. N.; Mehrotra, V.; Russell, M. W.; Huffman, D. R. *Science* **1992**, *257*, 219.
(5) Koch, A. J.; Becker, J. J. *J. Appl. Phys.* **1968**, *39*, 1261.
(6) Bean, C. P.; Livingston, J. D. *J. Appl. Phys.* **1959**, 120S.
(7) Sorensen, C. M. Magnetism. In *Nanoscale Materials in Chemistry*; Klabunde, K. J., Ed.; John Wiley & Sons, Inc.: New York, 2001; p169.
(8) Zboril, R.; Mashlan, M.; Petridis, D. *Chem. Mater.* **2002**, *14*, 969.
(9) Zhang, L.; Papaefthymiou, G. C.; Ying, J. Y. *J. Appl. Phys.* **1997**, *81*, 6892.
(10) Sartoratto, P. P. C.; Caiado, K. L.; Pedroza, R. C.; da Silva, S. W.; Morais, P. C. *J. Alloy Compd.* **2007**, *434*, 650.

10.1021/cm803153m CCC: $40.75
Published on Web 04/23/2009

photodynamic therapy.[11] The core Fe_3O_4 serves as a contrast agent for MRI. The Ir complex is suitable for phospohorescence imaging and $^1O_2$ production (for cancer treatment), while the silica shell encapsulates the Ir complex to ensure biocompatibility. Organically coated superparamagnetic iron oxide nanoparticles are commercially available and FDA-approved for MRI to aid in the diagnosis of cancer and cardiovascular diseases.[12,13] Nanoparticles are advantageous for such applications as their half-life in blood is extended by the reduced uptake by macrophages of the reticuloendothelial system especially in the liver and the spleen.[13] Thus, the uptake by macrophages of the lymph nodes increases where they can serve as contrast-enhancing agents.

Many studies have been devoted to the incorporation of Fe_xO_y nanoparticles in polymers to obtain superparamagnetic, transparent nanocomposites.[4,14] Silica coating of maghemite facilitates the homogeneous distribution of the nanoparticles in a polymer matrix, e.g., in thermoplastic shape-memory polymers.[15] The shape-memory effect of the composite can be triggered by inductive heating in an alternating magnetic field.

Gupta and Gupta[1] point out the importance of controlling both iron oxide core particle properties (e.g., size distribution, shape, and crystallinity) and surface characteristics that play a significant role in biokinetics and biodistribution of the nanoparticles. Typically, iron oxide nanoparticles are coated with SiO_2 by a sol−gel process[9,16,17] that involves several steps because Fe_xO_y core particle synthesis and their SiO_2 coating are essentially two separate unit operations.

An alternative process for the scalable manufacture of nanoparticles is offered by flame technology. This process can produce a wide variety of functional nanostructured materials with closely controlled properties.[18] The scalability of flame spray pyrolysis (FSP) has been demonstrated for pure[19] and mixed oxide[20] materials with production rates up to 1 kg/h. Maghemite particles 3−10 nm in diameter embedded in silica have been produced in premixed atmospheric[21,22] or low-pressure flames[23] and by FSP[24] in a single step. Commercially available MagSilica by Evonik Industries (formerly Degussa)[25] are also made by flame technology. These flame-made particles typically consist of several, small maghemite nanoparticles embedded in larger silica particles or aggregates.[21−24] However, the magnetic core size decreases by the presence of Si during Fe_xO_y formation.[24] Furthermore, relatively large amounts of silica must be added to ensure complete encapsulation of the core maghemite particles. The reduction of Fe_xO_y particle size by adding relatively large amounts (up to 79 wt % of Fe_2O_3) of nonmagnetic SiO_2 significantly decreases the magnetic performance of these composite materials. In contrast, sol−gel coating results in maghemite particles individually coated by thin SiO_2 layers, preserving their magnetization performance to a large extent.[24] Clearly, it is important to develop a scalable process for the synthesis of maghemite particles encapsulated by thin SiO_2 layers, thereby minimizing the nonmagnetic silica content of these particles. In addition, individual Fe_xO_y particles coated by thin SiO_2 layers rather than embedded in a continuous SiO_2 matrix[21−24] improves performance as well as the dispersion and incorporation of these materials in liquid or polymer matrixes.

In this work, an enclosed FSP reactor is used for the synthesis and in situ SiO_2 coating of Fe_2O_3 nanoparticles.[26] The process had been developed for SiO_2 coating and deactivation of photocatalytically active TiO_2 nanoparticles.[26,27] Iron oxide core nanoparticles are formed by FSP[28] of 0.34 M iron(III) acetylacetonate ($Fe(acac)_3$) in xylene/acetonitrile solutions (3:1 by volume).[24] Downstream from the FSP reactor, the freshly formed iron oxide aerosol is mixed with the coating precursor vapor (hexamethyldisiloxane: HMDSO) that is delivered in a swirling mode[27] and oxidized to form thin SiO_2 films onto the iron oxide particles. Uniformly SiO_2-coated Fe_xO_y particles are formed by optimizing process conditions[26] such as HMDSO vapor injection height and concentration and mixing intensity[27] with the Fe_xO_y core particle aerosol with a minimum number of separate SiO_2 and uncoated core particles.

Experimental Section

Particle Synthesis. Particles were produced in an enclosed FSP reactor described in detail elsewhere.[26,27] Precursor solutions, in all cases 0.34 M in total Fe metal concentration, were fed at 5 mL/min and dispersed by 5 L/min O_2 (Pan Gas, purity >99%). The solution spray was ignited by a methane/oxygen (1.5/3.2, total 4.7 L/min) premixed ring-shaped flame and the pressure drop at the nozzle tip was maintained at 1.5 bar.[29] The FSP reactor was enclosed by a 20 cm long quartz glass tube and the spray flame was sheathed by 40 L/min O_2 flowing through the outermost sinter metal plate

(11) Lai, C. W.; Wang, Y. H.; Lai, C. H.; Yang, M. J.; Chen, C. Y.; Chou, P. T.; Chan, C. S.; Chi, Y.; Chen, Y. C.; Hsiao, J. K. *Small* **2008**, *4*, 218.
(12) www.amagpharma.com, AMAG Pharmaceuticals, USA, accessed 06.10.2008.
(13) Josephson, L. Magnetic nanoparticles for MR imaging. In *BioMEMS and Biomedical Nanotechnology*; Ferrari, M., Ed.; Springer: New York, 2006; Vol. 1, p 227.
(14) Sohn, B. H.; Cohen, R. E. *Chem. Mater.* **1997**, *9*, 264.
(15) Mohr, R.; Kratz, K.; Weigel, T.; Lucka-Gabor, M.; Moneke, M.; Lendlein, A. *Proc. Natl. Acad. Sci. U. S. A.* **2006**, *103*, 3540.
(16) Yonemochi, Y.; Iijima, M.; Tsukada, M.; Jiang, H.; Kauppinen, E. I.; Kimata, M.; Hasegawa, M.; Kamiya, H. *Adv. Powder Technol.* **2005**, *16*, 621.
(17) Ma, D. L.; Veres, T.; Clim, L.; Normandin, F.; Guan, J. W.; Kingston, D.; Simard, B. *J. Phys. Chem. C* **2007**, *111*, 1999.
(18) Strobel, R.; Pratsinis, S. E. *J. Mater. Chem.* **2007**, *17*, 4743.
(19) Mueller, R.; Madler, L.; Pratsinis, S. E. *Chem. Eng. Sci.* **2003**, *58*, 1969.
(20) Jossen, R.; Mueller, R.; Pratsinis, S. E.; Watson, M.; Akhtar, M. K. *Nanotechnology* **2005**, *16*, S609.
(21) Zachariah, M. R.; Aquino, M. I.; Shull, R. D.; Steel, E. B. *Nanostruct. Mater.* **1995**, *5*, 383.
(22) McMillin, B. K.; Biswas, P.; Zachariah, M. R. *J. Mater. Res.* **1996**, *11*, 1552.
(23) Janzen, C.; Knipping, J.; Rellinghaus, B.; Roth, P. *J. Nanoparticle Res.* **2003**, *5*, 589.
(24) Li, D.; Teoh, W. Y.; Selomulya, C.; Woodward, R. C.; Amal, R.; Rosche, B. *Chem. Mater.* **2006**, *18*, 6403.
(25) Gottfried, H.; Janzen, C.; Pridoehl, M.; Roth, P.; Trageser, B.; Zimmermann, G. *Superparamagnetic oxidic particles, processes for their production and their use.* U.S. Patent 2003/0059603 A1, 2003.
(26) Teleki, A.; Heine, M. C.; Krumeich, F.; Akhtar, M. K.; Pratsinis, S. E. *Langmuir* **2008**, *24*, 12553.
(27) Teleki, A.; Buesser, B.; Heine, M. C.; Krumeich, F.; Akhtar, M. K.; Pratsinis, S. E. *Ind. Eng. Chem. Res.* **2009**, *48*, 85.
(28) Madler, L.; Kammler, H. K.; Mueller, R.; Pratsinis, S. E. *J. Aerosol Sci.* **2002**, *33*, 369.
(29) Madler, L.; Stark, W. J.; Pratsinis, S. E. *J. Mater. Res.* **2002**, *17*, 1356.

at the FSP burner.[26] At the top of that tube, a stainless steel metal torus pipe ring with 16 radial equispaced openings was positioned and the reactor was terminated by another 30 cm long quartz tube.[26]

Pure Fe_2O_3 was produced from 0.34 M in total Fe concentration precursor solutions of iron(III) acetylacetonate ($Fe(acac)_3$, Fluka, purity >97%) in xylene (Riedel-de Haën, puriss) and acetonitrile (Riedel-de Haën, puriss) at 3:1 volume ratio.[24] These particles were in situ coated with SiO_2 (SiO_2-coated Fe_2O_3) by introducing N_2 carrying its precursor, hexamethyldisiloxane (HMDSO, Aldrich, purity >98%), vapor from a bubbler at 10 °C along with additional 15 L/min mixing N_2 gas through the above metal torus pipe ring.[27] The silica content in the product powder (defined as $m_{SiO_2}/(m_{Fe_2O_3} + m_{SiO_2})$ varied from 6.5 to 46 wt % by controlling the N_2 flow rate through the HMDSO bubbler (0.08−0.97 L/min).

Co-oxidized particles (SiO_2/Fe_2O_3) were made also by FSP by adding HMDSO to the $Fe(acac)_3$ precursor solutions to result in 6.5−46 wt % SiO_2.[24] The total Fe concentration was kept at 0.34 M, while the Si concentration and thus the total mass production rate were varied. Also 15 L/min N_2 was injected though the torus ring but without HMDSO.[26] Particles formed by injecting HMDSO vapor downstream of the burner (in situ silica coating of FSP-made Fe_2O_3 particles) are denoted as SiO_2-coated Fe_2O_3 in contrast to SiO_2/Fe_2O_3, which refers to particles that were made by FSP co-oxidation of their precursors.

Particle Characterization. Product powders were analyzed by transmission electron microscopy (TEM), X-ray diffraction (XRD), and nitrogen adsorption at 77 K.[26] The primary particle size (d_{TEM}) distribution was measured by counting 979 particles of pure Fe_2O_3 and 303 particles of 23 wt % SiO_2-coated Fe_2O_3 using ImageJ software. The SiO_2 coating quality was assessed by chemisorption of isopropanol recording the thermal conductivity (TC) of the off-gases.[30] The dispersibility of suspensions was estimated by measuring size distributions in aqueous suspensions by dynamic light scattering (DLS, Malvern Zetasizer Nano series). Aqueous suspensions were prepared by 10 mg of powder in 20 mL of distilled water (Milli-Q) and ultrasonicated for 5 min (Sonics & Materials, Inc., Vibra Cell VCX 600, pulsed 0.1 s with 0.1 s pauses, each pulse corresponding to about 50 W). In total, three DLS measurements were taken right after ultrasonication and averaged, each consisting of 25 runs, 10 s per run. The measured intensity distributions were converted to volume distributions by applying the Mie-theory (Dispersion Technology Software, Version 4.2, Malvern). The particle magnetization was recorded on a MicroMag 3900 vibrating sample magnetometer at room temperature (VSM, Princeton Measurements Corporation).

Results and Discussion

Particle Properties. Figure 1 shows transmission electron micrograph (TEM) images at low (a) and high (b) magnification of pure, mostly hexagonal Fe_2O_3 particles. Silica coating of these maghemite particles was achieved by injecting HMDSO at various concentrations at 20 cm above the FSP burner. Figure 1 also shows images of these 23 wt % SiO_2-coated Fe_2O_3 at low (c) and high (d) TEM magnification. At higher magnification (Figure 1d) homogeneous and thin amorphous SiO_2 layers around Fe_2O_3 particles could be distinguished. No clear difference in the state of aggregation (chemical bonds) or agglomeration (physical bonds) could be distinguished between the

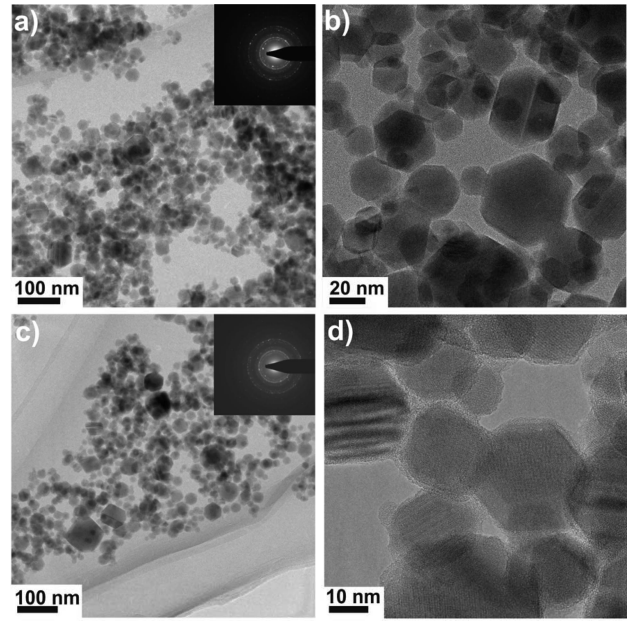

Figure 1. TEM images at low and high magnification of pure Fe_2O_3 (a,b) and 23 wt % SiO_2-coated Fe_2O_3 (c,d). Electron diffraction patterns are shown in the insets.

uncoated (Figure 1a) and coated (Figure 1c) Fe_2O_3 particles as has been demonstrated for TiO_2 nanoparticles made in vapor- and liquid-fed flame reactors.[31]

For comparison, SiO_2/Fe_2O_3 particles were also made by FSP co-oxidation of solutions containing HMDSO and $Fe(acac)_3$ in the enclosed reactor. In SiO_2/Fe_2O_3 (Figure 2a), crystalline iron oxide particles are segregated to the edge of amorphous SiO_2 particles,[24] similar to FSP-made[26] SiO_2/TiO_2. Figure 2 also shows images of 6.5 (b) and 23 wt % (c) SiO_2-coated Fe_2O_3 particles at even higher TEM magnification. The lattice planes with a spacing of 3.0 Å are visible in the 6.5 wt % SiO_2-coated Fe_2O_3 particle, corresponding to the (220) plane of γ-Fe_2O_3 (maghemite, PDF: 00-039-1346). An amorphous fringe could not be observed at 6.5 wt % SiO_2 (Figure 2b), as this silica content would correspond to a theoretical coating thickness of <1 nm on a 22 nm spherical Fe_2O_3 particle.[30] However, the addition of 23 wt % SiO_2 results in an amorphous film about 2 nm thick (Figure 2c), in good agreement with the theoretically expected coating thickness of 2 nm. These particles are similar to those obtained by sol−gel coating of maghemite with 43 wt % SiO_2.[24] The formation of silica coatings by this in situ FSP coating process has already been verified by numerous characterization techniques.[30] Traces of carbon from combustion could be present; however, they are low at the employed high temperatures and highly oxidative conditions, as has been shown in flame synthesis of dental prosthetic materials.[32] Grimm et al.[33] reported on a carbon content of 1.7 wt % of FSP-made Fe_2O_3 from $Fe(acac)_3$ in toluene precursor solutions. However, traces of carbon would not have a negative impact in biomedical applications, as studies have also focused on *biocompatible* carbon coatings on magnetic nanoparticles.[1]

(30) Teleki, A.; Akhtar, M. K.; Pratsinis, S. E. *J. Mater. Chem.* **2008**, *18*, 3547.
(31) Teleki, A.; Wengeler, R.; Wengeler, L.; Nirschl, H.; Pratsinis, S. E. *Powder Technol.* **2008**, *181*, 292.
(32) Schulz, H.; Pratsinis, S. E.; Rugger, H.; Zimmermann, J.; Klapdohr, S.; Salz, U. *Colloid Surf., A* **2008**, *315*, 79.
(33) Grimm, S.; Stelzner, T.; Leuthausser, J.; Barth, S.; Heide, K. *Thermochim. Acta* **1997**, *300*, 141.

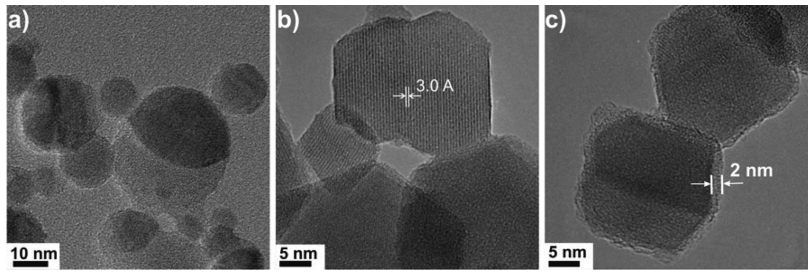

Figure 2. TEM images of co-oxidized 23 wt % SiO_2/Fe_2O_3 (a), 6.5 wt % SiO_2-coated Fe_2O_3 (b), and 23 wt % SiO_2-coated Fe_2O_3 (c).

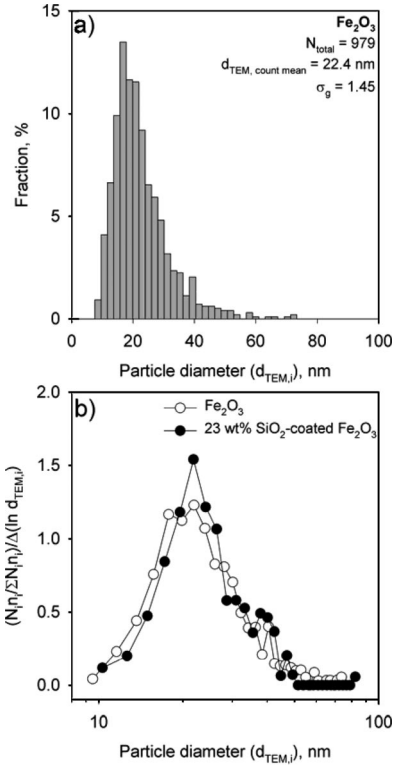

Figure 3. Histogram (a) and primary particle number size distribution (b) of Fe_2O_3 (open circles) and 23 wt % SiO_2-coated Fe_2O_3 (filled circles).

Figure 3a shows a histogram of the primary particle size (d_{TEM}) distribution of pure Fe_2O_3 obtained from TEM images. The count mean diameter from TEM analysis was 22.4 nm and slightly smaller than the grain size d_{BET} of 24 ± 1 nm (with $\rho_{\gamma\text{-}Fe_2O_3} = 4.9$ g/cm^3) calculated from the specific surface area assuming spherical particles (SSA = 51 ± 2 m^2/g). This difference might stem from the hexagonal shape of the particles but is also typical for unimodal, self-preserving particle size distributions and the difference[34,35] between the two average diameters: number (TEM) and Sauter (BET). These particles are larger than those made in open FSP reactors[36] where heat is rapidly dissipated, thus reducing the high-temperature particle residence time and sintering and preventing particle growth. Figure 3b shows the primary particle number size distributions of Fe_2O_3 (open circles) and 23 wt % SiO_2-coated Fe_2O_3 (filled circles) particles as calculated from the histograms (e.g., Figure 3a) from TEM analysis. The distribution is slightly shifted to larger sizes for SiO_2-coated Fe_2O_3 compared to that for the uncoated particles, possibly due to the thin coatings formed that increase the particle diameter (Figure 2c). The count mean diameter was 22.9 nm for the 23 wt % SiO_2-coated particles and thus lower than the 4 nm increase as expected from the mass balance. The geometric standard deviation σ_g, which describes the width of the primary particle size distribution, was 1.45 for uncoated Fe_2O_3 and corresponds to self-preserving size distributions.[34] It was slightly narrower, $\sigma_g = 1.39$, for the SiO_2-coated particles as condensation (here by silica) narrows the aerosol size distribution below its self-preserving limit.[37] As rather narrow particle size distributions are preferred for biomedical applications,[1] particle size distributions could be further narrowed by ionic additives during combustion.[38]

X-ray diffraction (XRD) indicates that the present FSP-made iron oxide particles (Figure 4a) are γ-Fe_2O_3 (maghemite, cubic; PDF: 00-039-1346) along with α-Fe_2O_3 (hematite, rhombohedral; PDF: 01-087-1165, (104) plane at $2\theta = 33°$), in agreement with premixed flame synthesis of iron oxide.[21,39] The presence of Fe_3O_4 (magnetite) cannot be ruled out by XRD as maghemite and magnetite patterns are nearly identical.[21] However, the oxygen-rich environment in the flame reactor and the reddish-brown color of these powders suggest formation of γ-Fe_2O_3. The α-Fe_2O_3 phase forms because higher temperatures are afforded in the enclosed[40] (as opposed to open) FSP reactors.[36] Note that γ-Fe_2O_3 transforms to α-Fe_2O_3 at higher temperatures (50 wt % α-Fe_2O_3 obtained after 70 min at 450 °C in air with d_{XRD} = 9 nm γ-Fe_2O_3 starting material),[41] however with a strong dependence on initial particle size.[8] The crystalline phase of FSP-made iron oxides could be further controlled by varying the fuel-to-air ratio during combustion and by the valence state of the applied Fe precursor.[42] The (311) plane of γ-Fe_2O_3 located at $2\theta = 35.7°$ was used to calculate the crystallite size using TOPAS 3 software. For pure γ-Fe_2O_3, the diameter is 14 ± 0.8 nm, which is smaller than d_{BET} and

(34) Hinds, C. W., *Aerosol Technology: Properties, behavior and measurement of airborne particles*; John Wiley & Sons, Inc.: New York, 1982.
(35) Kammler, H. K.; Jossen, R.; Morrison, P. W.; Pratsinis, S. E.; Beaucage, G. *Powder Technol.* **2003**, *135*, 310.
(36) Li, D.; Teoh, W. Y.; Selomulya, C.; Woodward, R. C.; Munroe, P.; Amal, R. *J. Mater. Chem.* **2007**, *17*, 4876.
(37) Pratsinis, S. E. *J. Colloid Interface Sci.* **1988**, *124*, 416.
(38) Xiong, Y.; Pratsinis, S. E.; Mastrangelo, S. V. R. *J. Colloid Interface Sci.* **1992**, *153*, 106.
(39) Janzen, C.; Roth, P.; Rellinghaus, B. *J. Nanoparticle Res.* **1999**, *1*, 163.
(40) Teleki, A.; Pratsinis, S. E.; Kalyanasundaram, K.; Gouma, P. I. *Sens. Actuators, B* **2006**, *119*, 683.
(41) Belin, T.; Millot, N.; Bovet, N.; Gailhanou, M. *J. Solid State Chem.* **2007**, *180*, 2377.
(42) Strobel, R.; Pratsinis, S. E. *Adv. Powder Technol.* **2009**, doi: 10.1016/j.apt.2008.08.002.

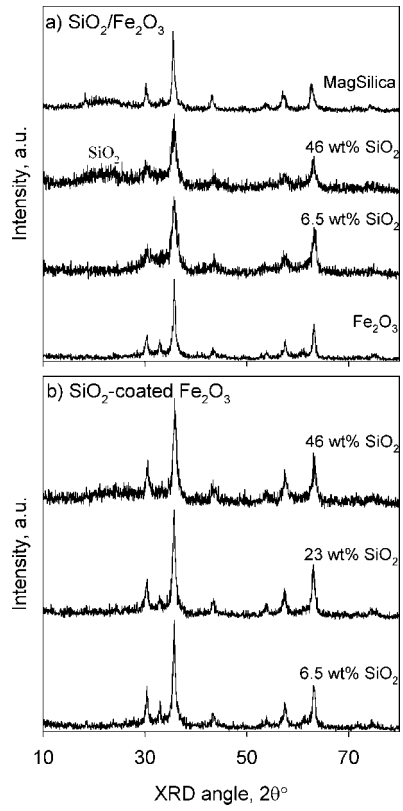

Figure 4. XRD spectra of pure Fe_2O_3 and co-oxidized SiO_2/Fe_2O_3 (a) and SiO_2-coated Fe_2O_3 (b).

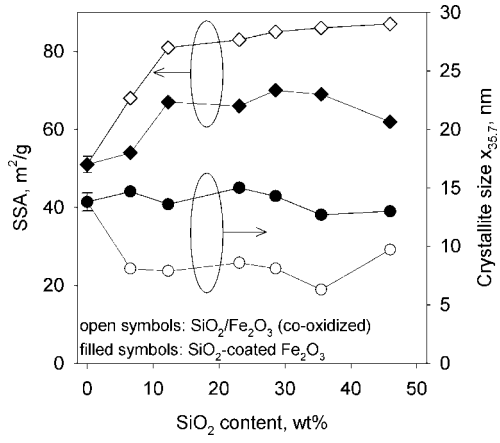

Figure 5. Specific surface area (SSA, diamonds) and Fe_2O_3 crystallite size (circles) as a function of SiO_2 content for SiO_2/Fe_2O_3 (open symbols) and SiO_2-coated Fe_2O_3 (filled symbols) particles.

d_{TEM} (Figure 3a), indicating polycrystalline particles in agreement with microscopy (Figure 1a).

The effect of SiO_2 content on Fe_2O_3 size and crystallinity was investigated because silica can promote certain phases (anatase for TiO_2) and reduce crystallite or grain size in hot-wall[43] or flame[44] reactors. Figure 4 shows XRD spectra of co-oxidized SiO_2/Fe_2O_3 (a) and SiO_2-coated Fe_2O_3 (b). Figure 5 shows the impact of SiO_2 on SSA (diamonds) and Fe_2O_3 crystallite size (circles) on co-oxidized SiO_2/Fe_2O_3 (open symbols) or SiO_2-coated Fe_2O_3 (filled symbols) particles. For SiO_2/Fe_2O_3, the SSA increases and crystallite size decreases by addition of SiO_2, especially at low SiO_2 contents (Figure 5).[24] The silica matrix formed by Si/Fe precursor co-oxidation is evident at high SiO_2 contents (46 wt %) as an amorphous "hump" in the XRD spectra (Figure 4a) and results in the highest SSA compared to that of pure Fe_2O_3 (Figure 5). The silica structure also inhibits crystallite growth by coagulation and sintering in the flame as evidenced by the nearly constant (but small) Fe_2O_3 crystallite size of 8 nm at all SiO_2 contents (Figure 5). The α-Fe_2O_3 could not be distinguished at any SiO_2 content in the XRD spectra (Figure 4a), either due to the small crystallite size which causes peak broadening or the suppression of this phase in the presence of silica.[23] Small grain sizes favor γ-Fe_2O_3 and prevent α-Fe_2O_3 formation below a critical size ($\sim$15 nm).[41]

In contrast, the FSP in situ coating process allows independent control of core particle size and SiO_2 coating film thickness. The crystallite size of SiO_2-coated Fe_2O_3 particles remains constant even at high SiO_2 contents (Figure 5) as HMDSO is added after Fe_2O_3 particle formation and growth has ceased in the flame.[26] In the XRD spectra of SiO_2-coated Fe_2O_3 also the (104) plane of α-Fe_2O_3 was visible up to 23 wt % SiO_2 (Figure 4b) in contrast to that of SiO_2/Fe_2O_3 particles (Figure 4a). The SSA slightly increases at low SiO_2 contents, probably by formation of solid solutions at these low Si concentrations as routinely seen in flame synthesis of mixed SiO_2 oxides.[44] The SSA is rather constant at $\geq$12 wt % SiO_2 and slightly decreases at higher SiO_2 contents as larger particles are formed by thicker coatings (Figure 5).

The dispersibility of aqueous particle suspensions of these particles was measured by dynamic light scattering (DLS). Pure Fe_2O_3 particles exhibited a trimodal distribution of broadly distributed agglomerates (30−5000 nm). In contrast, 23 wt % SiO_2-coated Fe_2O_3 exhibited a unimodal distribution of particles 50−200 nm. This distribution was narrower than the bimodal distributions (40−5000 nm) of co-oxidized 23 wt % SiO_2/Fe_2O_3 and commercial MagSilica (SSA = 57 m^2/g, $x_{35.7}$ = 18.6 nm) and 100−5000 nm by DLS here. These data show that silica coatings of individual iron oxide nanoparticles drastically minimize their degree of agglomeration. The strong agglomeration observed for uncoated Fe_2O_3 or partially coated SiO_2/Fe_2O_3 here could stem from attraction of the magnetic cores. Further, the ζ potential of Fe_2O_3 is close to zero at pH 7 (isoelectric point), which causes strong agglomeration.[45] In contrast, the isoelectric point of pure SiO_2 is around pH 1.7,[30,45] thus improving the dispersibility of SiO_2-coated Fe_2O_3 particles in water. The presence of large agglomerates in SiO_2/Fe_2O_3 thus also indicates the presence of some uncoated Fe_2O_3 particles while for MagSilica it is known that each particle contains several Fe_2O_3 nanoparticles coated with silica though some uncoated might be present.

The coating quality was investigated more specifically by isopropanol chemisorption.[30] This method relies on the difference in isopropanol surface adsorption between SiO_2 and Fe_2O_3.[46] The number of active surface sites for isopropanol adsorption on SiO_2 and Fe_2O_3 is 0.5 and 7.9 μmol/m^2,

(43) Akhtar, M. K.; Pratsinis, S. E.; Mastrangelo, S. V. R. *J. Am. Ceram. Soc.* **1992**, *75*, 3408.
(44) Vemury, S.; Pratsinis, S. E. *J. Am. Ceram. Soc.* **1995**, *78*, 2984.
(45) Parks, G. A. *Chem. Rev.* **1965**, *65*, 177.
(46) Kulkarni, D.; Wachs, I. E. *Appl. Catal., A* **2002**, *237*, 121.

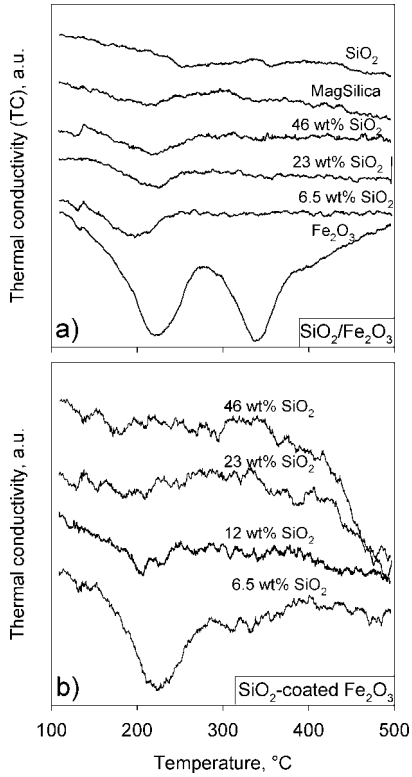

Figure 6. Off-gas thermal conductivity as a function of temperature during isopropanol desorption from pure SiO_2[30] and Fe_2O_3, co-oxidized SiO_2/Fe_2O_3 (a) and SiO_2-coated Fe_2O_3 (b) particles with different SiO_2 contents.

respectively.[46] Thus, isopropanol is allowed to chemisorb on the particle surface at 110 °C. The particles are then continuously heated to 500 °C in helium, and the thermal conductivity (TC) of the off-gas is recorded. Isopropanol or surface reaction products (e.g., acetone or propene[46]) evaporating from the particle reduce the TC. Figure 6a shows the TC as a function of temperature for pure SiO_2 and Fe_2O_3. Silica hardly chemisorbs isopropanol and no sharp drop in TC can be observed at any temperature.[30] In contrast, two TC peaks are detected for Fe_2O_3: one at 221 °C and a second at 334 °C. The first can be attributed to the release of adsorbed isopropanol or surface reaction products as it corresponds well with the surface isopropoxide decomposition temperature of 231 °C.[46] The second might stem from release of further surface species or even from a partial transformation of γ-Fe_2O_3 to Fe_3O_4. Grimm et al.[33] observed the reduction of Fe_2O_3 made by FSP of $Fe(acac)_3$ precursor solution at 370 °C under argon. They attributed this to the reaction with surface-reductive adsorbates, i.e., carboxylate, that would release CO_2.[33,47]

Figure 6a also shows the TC for co-oxidized SiO_2/Fe_2O_3 with 6.5, 23, and 46 wt % SiO_2 and commercially available MagSilica. At all SiO_2 contents a peak for the desorption of isopropanol is visible, implying that part of the Fe_2O_3 particle surface is accessible for isopropanol chemisorption. Thus, co-oxidation of Si/Fe precursors even at high SiO_2 contents does not result in a complete or hermetic encapsulation of Fe_2O_3 particles, an essential requirement for biological or nanocomposite applications.[1] This was also shown by acid dissolution of similar SiO_2/Fe_2O_3 particles made by FSP co-oxidation, even with 79 wt % SiO_2.[24] Figure 6a also shows the TC for MagSilica with a slight desorption of isopropanol that indicates imperfect silica coating by flame co-oxidation.[23,25] The second peak at the higher temperature observed for pure γ-Fe_2O_3 was not visible for any of the SiO_2-containing particles, indicating that SiO_2 may have prevented the phase transformation to Fe_3O_4.

Figure 6b shows TC signals for SiO_2-coated Fe_2O_3 particles with 6.5, 12, 23, and 46 wt % SiO_2. The peak of isopropanol desorption is visible at 6.5 wt % SiO_2, slightly distinguishable at 12 wt % SiO_2, and no longer discernible at ≥23 wt % SiO_2. This suggests that >12 wt % is the threshold value for hermetic or continuous coatings. Similarly, acid dissolution tests of sol−gel-made SiO_2-coated Fe_2O_3 show a complete encapsulation of the core particles.[24]

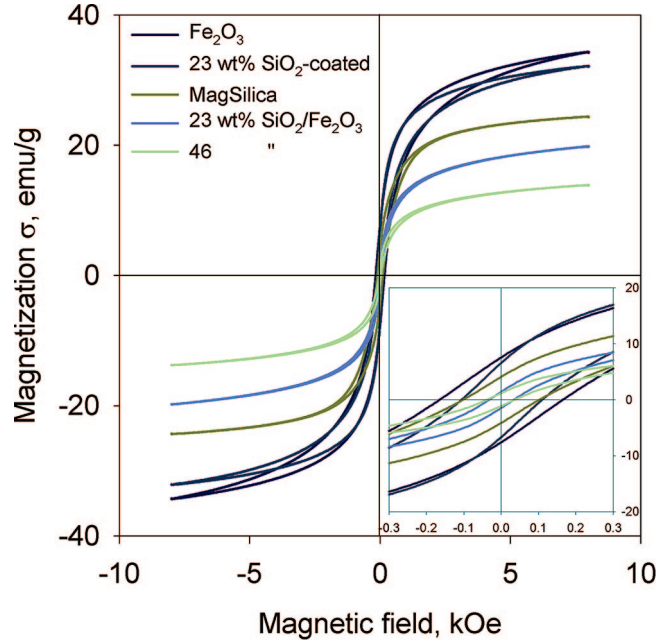

Figure 7. Magnetization (σ) as a function of the applied magnetic field for pure Fe_2O_3, co-oxidized SiO_2/Fe_2O_3, MagSilica, and SiO_2-coated Fe_2O_3. The inset shows a magnification at low magnetic fields highlighting the coercivity and remanence of the particles (Table 1).

Table 1. Magnetization (σ) at 8 kOe, Coercivity (H_c), and Remanence (M_r) of Pure, SiO_2-Coated, and Co-oxidized Fe_2O_3 Particles

	σ at 8 kOe	$\sigma_{Fe_2O_3}$ at 8 kOe[a]	H_c (kOe)	M_r (emu/g)
Fe_2O_3	34	34	0.16	7.7
23 wt % SiO_2-coated Fe_2O_3	32	42	0.1	6.6
MagSilica	24		0.1	4.1
23 wt % SiO_2/Fe_2O_3	20	26	0.03	1.5
46 wt % SiO_2/Fe_2O_3	14	26	0.03	1.2

[a] $\sigma_{Fe_2O_3}$ was calculated per unit mass of γ-Fe_2O_3 in the samples.

Magnetic Properties. Figure 7 shows the magnetization of flame-made Fe_2O_3 nanoparticles measured by a vibrating sample magnetometer (VSM). Table 1 shows the magnetization at 8 kOe (corresponding to 0.8 T in free space)[7] and the corresponding coercivity and remanence data. These iron oxide nanoparticles exhibit nearly zero hysteresis as expected and shown by the inset of Figure 7. At the maximum applied magnetic field, nearly all particles have reached their

(47) Grimm, S.; Schultz, M.; Barth, S.; Muller, R. *J. Mater. Sci.* **1997**, *32*, 1083.

saturation magnetization; only for Fe_2O_3 and SiO_2-coated Fe_2O_3 a slight increase could be expected at higher magnetic fields. The highest magnetization corresponds to pure Fe_2O_3, as expected (Figure 1b). The reported saturation magnetization of bulk maghemite is about 80 emu/g.[48] The lower value obtained here for the γ-Fe_2O_3 nanoparticles could be attributed to the presence of hematite[49] and reduced particle size.[1]The first studies on the decrease of magnetization in γ-Fe_2O_3 attributed this phenomena to the existence of noncollinear spins at the surface of nanoparticles.[50] However, apart from these magnetically disordered surface layers, it has also been shown that the degree of structural disorder in the bulk will affect the magnetic behavior of the nanoparticles.[48,51]

The addition of 23−46 wt % SiO_2 reduces the magnetization by the presence of silica[9,24] and the reduction of Fe_2O_3 crystallite size for SiO_2/Fe_2O_3 particles (Figure 5).[5] In contrast, the magnetization of 23 wt % SiO_2-coated Fe_2O_3 is very close to pure Fe_2O_3 and higher than that of MagSilica, which is in agreement with that reported earlier of 22−32 emu/g saturation magnetization.[15] This demonstrates that Fe_2O_3 nanoparticles coated in situ by thin SiO_2 films retain most of their magnetic properties. The coercivity and remanence of all samples is low (Table 1), indicating superparamagnetism. Both properties decrease with the addition of silica, more for co-oxidized particles and less for SiO_2-coated Fe_2O_3. The slight hysteresis of the magnetization curves might stem from a ferromagnetic contribution of blocked particles as observed typically by low-temperature magnetic measurements.[2,23,24] Table 1 also shows the magnetization accounting only for the mass of Fe_2O_3 in the samples at 8 kOe. Co-oxidized SiO_2/Fe_2O_3 exhibits low values of magnetization, independent of silica content in agreement with their constant, small crystallite sizes (Figure 5). In contrast, 23 wt % SiO_2-coated Fe_2O_3 has a higher magnetization compared to that of uncoated Fe_2O_3 (Table 1). This enhancement in magnetization could stem from a lower hematite content[49] in the coated particles compared to that of the uncoated ones (Figure 4) or from differences in aggregation/agglomeration and interparticle interactions[52] of coated and uncoated particles.

The SiO_2-dominated surface shifts the isoelectric point of coated and co-oxidized particles to pH 1−3, in contrast to that of pH 7 for pure Fe_2O_3.[24] This low isoelectric point facilitates the dispersion of such particles in aqueous solutions even in the absence of surfactants. Figure 8 shows a ferrofluid prepared from 23 wt % SiO_2-coated Fe_2O_3 (Figure 1c,d) suspended in water in the absence (a) and presence (b) of a magnetic field. The superparamagnetic properties can be observed as the fluid returns to the state shown in Figure 8a after removal of the magnet. Such suspensions can facilitate the contrast of MRI as they interact with external magnetic fields and can be positioned in a specific area.[1] Thus, the FSP in situ coating process enables complete encapsulation of Fe_2O_3 nanoparticles at relatively low SiO_2 contents, resulting in highly superparamagnetic Fe_2O_3 particles (Figure 7, Table 1) at reduced cost (as less Si is needed compared to co-oxidized products).

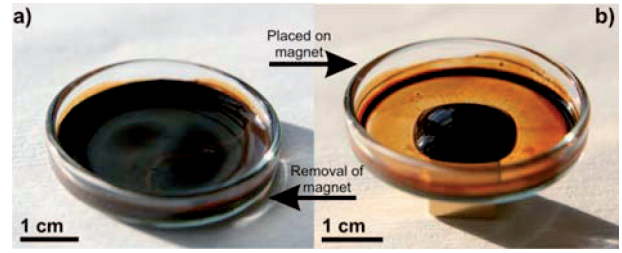

Figure 8. Ferrofluid containing 200 g/L of 23 wt % SiO_2-coated Fe_2O_3 nanoparticles in the absence (a) and presence (b) of a NdFeB magnet (0.35 T at the surface, 12 × 12 × 12 mm).

Conclusions

A gas-phase process is presented for hermetic SiO_2 coating of γ-Fe_2O_3 nanoparticles exhibiting superparamagnetic properties close to those of pure iron oxide. The core γ-Fe_2O_3 particles were produced by scalable flame spray pyrolysis and coated in situ by thin, amorphous SiO_2 layers. The complete encapsulation of the core particles (22 nm) at >12 wt % SiO_2 was demonstrated by isopropanol chemisorption. The process enables independent control of core particle crystallinity and size along with silica-coating thickness. The silica content in the product can be minimized to decrease the negative impact of silica on the saturation magnetization of γ-Fe_2O_3. Also, these particles exhibited excellent dispersibility compared to that of flame-made co-oxidized silica−iron oxide and commercially available particles.

Acknowledgment. TEM analysis was performed at the Electron Microscopy Center of ETH Zurich (EMEZ). We thank A. M. Hirt at the Institute of Geophysics, ETH Zurich, for assistance with the VSM measurements.

CM803153M

(48) Dutta, P.; Manivannan, A.; Seehra, M. S.; Shah, N.; Huffman, G. P. *Phys. Rev. B* **2004**, *70*, 174428.
(49) Cannas, C.; Gatteschi, D.; Musinu, A.; Piccaluga, G.; Sangregorio, C. *J. Phys. Chem. B* **1998**, *102*, 7721.
(50) Coey, J. M. D. *Phys. Rev. Lett.* **1971**, *27*, 1140.
(51) Morales, M. P.; Veintemillas-Verdaguer, S.; Montero, M. I.; Serna, C. J.; Roig, A.; Casas, L.; Martinez, B.; Sandiumenge, F. *Chem. Mater.* **1999**, *11*, 3058.
(52) Pardoe, H.; Chua-anusorn, W.; St Pierre, T. G.; Dobson, J. *J. Magn. Magn. Mater.* **2001**, *225*, 41.